On the Varying Responses of East Asian Winter Monsoon to Three Types of El Niño: Observations and Model Hindcasts

JI-WON KIM,[a] TING-HUAI CHANG,[b] CHING-TENG LEE,[b] AND JIN-YI YU[a]

[a] *Department of Earth System Science, University of California, Irvine, California*
[b] *Central Weather Bureau, Taipei, Taiwan*

(Manuscript received 7 October 2020, in final form 19 January 2021)

ABSTRACT: Using observational data and model hindcasts produced by a coupled climate model, we examine the response of the East Asian winter monsoon (EAWM) to three types of El Niño: eastern Pacific (EP) and central Pacific I (CP-I) and II (CP-II) El Niños. The observational analysis shows that all three El Niño types weaken the EAWM with varying degrees of impact. The EP El Niño has the largest weakening effect, while the CP-II El Niño has the second largest, and the CP-I El Niño has the smallest. We find that diverse El Niño types impact the EAWM by altering the responses of two anomalous anticyclones during El Niño mature winter: the western North Pacific anticyclone (WNPAC) and Kuroshio anticyclone (KAC). The WNPAC responses are controlled by the Gill response and Indian Ocean warming processes that both respond to the eastern-to-central tropical Pacific precipitation anomalies. The KAC responses are controlled by a poleward wave propagation responding to the northwestern tropical Pacific precipitation anomalies. We find that the model hindcasts significantly underestimate the weakening effect during the EP and CP-II El Niños. These underestimations are related to a model deficiency in which it produces a too-weak WNPAC response during the EP El Niño and completely misses the KAC response during both types of El Niño. The too-weak WNPAC response is caused by the model deficiency of simulating too-weak eastern-to-central tropical Pacific precipitation anomalies. The lack of KAC response arises from the unrealistic response of the model's extratropical atmosphere to the northwestern tropical Pacific precipitation anomalies.

KEYWORDS: Asia; Pacific Ocean; Atmosphere-ocean interaction; El Niño; Model output statistics; Interannual variability

1. Introduction

The East Asian winter monsoon (EAWM) is a prominent circulation feature in the atmosphere, driven by the land–sea thermal contrast between the cold Eurasian continent and warm Pacific Ocean (e.g., Li 1955; Tao 1957). The prevailing surface northerly wind associated with the EAWM brings dry and cold conditions to the East Asian continent. Strong cold surge and heavy snowfall events can occur when the EAWM intensifies. Those events cause severe damage to crop and livestock productivity and socioeconomic activities over large areas of East Asian countries, such as eastern China, the Korean Peninsula, and Japan, as well as areas near the South China Sea (Wang 2006). The variations of EAWM can also affect climate and weather conditions far away, such as Madden–Julian oscillation activities over the tropical western Pacific (Chen et al. 2017). It is also reported that some significant EAWM variations can even impact surface air temperatures over North America via atmospheric teleconnections (Ma et al. 2018). For these reasons, extensive efforts have been made to understand EAWM variability and to improve its predictability (e.g., Chang et al. 1979; Chang and Lau 1982; Lau and Li 1984; Ding and Krishnamurti 1987; Ding 1994; Newman and Sardeshmukh 1998; Chan and Li 2004; Huang et al. 2003, 2007; Chang et al. 2006; Wang 2006; Wang et al. 2010; Chen et al. 2017; Ma et al. 2018).

Forcing from El Niño–Southern Oscillation (ENSO) is a major contributor to EAWM variability on interannual time scales (e.g., Zhang et al. 1996; Ji et al. 1997; Alexander et al. 2002; Chang et al. 2004; McPhaden et al. 2006; Sakai and Kawamura 2009; J. W. Kim et al. 2014, 2017; Li et al. 2017; Kim and An 2019). The intensity of EAWM tends to be weaker than normal during El Niño years. That is because El Niño events typically induce an anomalous anticyclone over the western North Pacific (WNPAC), which produces southerly wind anomalies in its western flank, weakening the prevailing EAWM-related northerly wind (e.g., B. Wang et al. 2000; Wang and Zhang 2002). However, this conventional view of the El Niño–EAWM relationship is currently being revised due to the recognition that El Niño has diverse types and their climate impacts can be different (e.g., Ashok et al. 2007; Kao and Yu 2009; Kug et al. 2009; Yeh et al. 2009; Yu et al. 2012a, 2017; Capotondi et al. 2015). El Niño events can be classified into two different types based on the zonal location of their maximum sea surface temperature (SST) anomalies. They are often referred to as the eastern Pacific (EP) El Niño and central Pacific (CP) El Niño, following Yu and Kao (2007) and Kao and Yu (2009). The EP El Niño has its maximum SST anomalies located in the tropical eastern Pacific, closer to the South American coast, while the CP El Niño has its maximum SST anomalies located in the tropical central Pacific, closer to the international date line. More recent studies suggested that the CP El Niño needs to be further divided into two subtypes due to differences in their temporal evolutions and climate impacts (Wang and Wang 2013). Here, we refer to these two subtypes as the CP-I and CP-II El Niños following Chen et al. (2019). The CP-I El Niño has its maximum SST anomalies that mostly originate and develop in the tropical central Pacific with a structure symmetric to the equator. The CP-II El Niño,

Corresponding author: Jin-Yi Yu, jyyu@uci.edu

DOI: 10.1175/JCLI-D-20-0784.1

besides having its maximum SST anomalies in the tropical central Pacific, is also characterized by significant SST anomalies spreading between the tropical central Pacific and south of North American coast. Hence, its SST anomaly structure is asymmetric with regard to the equator. The CP-I and CP-II El Niños have also been shown to produce different impacts on rainfall amounts in southern China, typhoon tracks over the western North Pacific, and SST variations in the tropical Indian Ocean and South China Sea (Wang and Wang 2013, 2014; Tan et al. 2016).

A recent study by Chen et al. (2019) found that these three types of El Niño (i.e., EP, CP-I, and CP-II types) produce distinct impacts on the WNPAC (cf. the western Pacific subtropical high in their study). As mentioned, the conventional view invokes the WNPAC to explain how El Niño can impact EAWM variability. It is thus plausible that the El Niño–EAWM relationship would likewise change depending on the El Niño types. Studies on the impact of each El Niño type on EAWM variability have mostly separated El Niño events into only the EP and CP types (e.g., Yuan et al. 2012; Gong et al. 2015; Shi and Qian 2018). In the present study, we therefore further separate CP El Niño events into the two subtypes to show that the EAWM responses are indeed different for the EP, CP-I, and CP-II types of El Niño in the observations. It is also important for contemporary climate models to properly simulate the various EAWM responses to different El Niño types so that they can produce skillful EAWM predictions using the El Niño information (e.g., Kang and Lee 2019; Chen et al. 2020). In this study, we also examine climate model hindcasts to understand how and why climate models can or cannot properly simulate EAWM responses to diverse El Niño types. We choose to analyze retrospective hindcast simulations produced by the Taiwan Central Weather Bureau Climate Forecast System 1-tiered model (TCWB1T model; cf. Wu et al. 2019) from the Central Weather Bureau (CWB) in Taiwan due to its availability to us. Because of the common model deficiencies shared by many other climate models, which we will elaborate on later, the results and findings obtained from the TCWB1T model can be applied to other climate models as well.

The remaining part of this manuscript is organized as follows. Section 2 describes the datasets and methodologies utilized in this study. In section 3, we examine the varying responses of EAWM to the three types of El Niño in the observations. Then, we identify the causes controlling the EAWM responses by invoking physical processes that impact the responses of WNPAC and another anomalous anticyclone near the Kuroshio Extension (sections 3a and 3b). In the following section (section 3c), we further examine the model hindcasts so as to see whether the model can simulate the observed EAWM responses to diverse El Niño types and reveal any model deficiencies that cause it to simulate EAWM responses differently from the observations. A summary and discussion of the main findings in this study is provided in section 4.

2. Data and methods

We used three observation/reanalysis products in this study. Monthly means of surface pressure P_s and zonal U and meridional V winds at the lower troposphere (i.e., 850-hPa level) were obtained from the National Centers for Environmental Prediction–Department of Energy Reanalysis 2 (NCEP–DOE R2; Kanamitsu et al. 2002), which are available from January 1979 to the present. Monthly means of precipitation (PRCP) were obtained from the Global Precipitation Climatology Project version 2.3 (GPCPv2.3; Adler et al. 2003), which are also available from January 1979 to the present. Monthly means of SST were obtained from the Hadley Center Sea Ice and Sea Surface Temperature version 1.1 (HadISSTv1.1; Rayner et al. 2003), which are available from January 1870 to the present. For the purpose of model evaluation, we only analyzed the data from January 1982 to December 2011 in this study. All data were interpolated to the grid points of the model hindcasts (i.e., $1° \times 1°$ global grids) to reduce uncertainties associated with different spatial resolutions.

We chose to analyze the hindcast outputs produced by the TCWB1T model. The TCWB1T model is an atmosphere–ocean coupled model, composed of the Global Forecast System in CWB as its atmospheric model component (Paek et al. 2015) and the third version of Modular Ocean Model as its oceanic model component (Pacanowski and Griffies 1998). The model hindcast period covers from January 1982 to December 2011. For each month, hindcasts were launched at days 1, 3, 6, 8, 11, 13, 16, 18, 21, and 23 to result in 10-member ensembles. The hindcast outputs were obtained from the monthly averages over the daily hindcasts, which are lead-0 to lead-5 for each ensemble member in each month. Thus, we have 10 ensembles of model hindcasts with lead months between 0 to 5 from January 1982 to December 2011.

Three climate indices were used to quantify the strengths of EAWM, WNPAC, and an extratropical anomalous anticyclone near the Kuroshio Extension [KAC, abbreviated from Kuroshio anticyclone following Son et al. (2014)]. The EAWM index used in this study is the same as the one defined by Yang et al. (2002), which was calculated using the boreal winter value of low-level meridional wind anomalies averaged within an East Asian region of 20–40°N and 100–140°E (note the boreal winter runs from December to the following February). The index value was normalized by its standard deviation (s.d.) and multiplied by −1 to become the EAWM index. After multiplication, a positive (negative) index value corresponds to a stronger (weaker) than normal EAWM intensity. This EAWM index is known to adequately capture the El Niño–induced southerly wind anomalies blowing along the east coast of East Asia (cf. J. W. Kim et al. 2017); therefore, it can properly reflect the influence of diverse El Niño types on the EAWM. The WNPAC index was defined as the boreal winter value of surface pressure anomalies averaged within a western North Pacific region (i.e., 5°–20°N, 120°–160°E; see solid rectangles in Fig. 2). The KAC index was defined in the same way as the WNPAC index except for an adjustment in the selected region to the Kuroshio Extension (i.e., 35°–50°N, 140°–160°E; see dashed rectangles in Fig. 2).

According to Chen et al. (2019), during the analysis period of 1982–2011, there were two EP El Niño events (1982/83 and 1997/98 events), three CP-I El Niño events (1987/88, 1990/91, and 2002/03 events), and four CP-II El Niño events (1991/92,

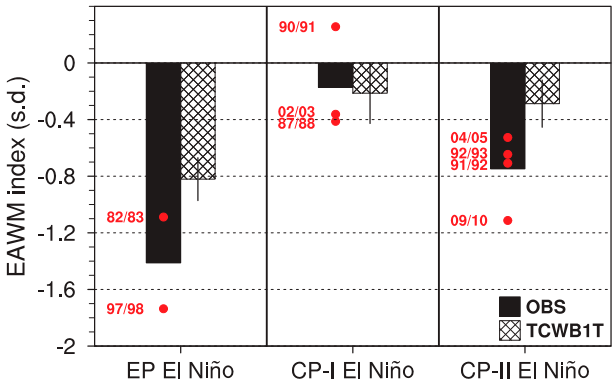

FIG. 1. Changes in the EAWM index (s.d.) composited for the three types of El Niño (i.e., EP, CP-I, and CP-II El Niños) for the observations (solid bar) and the TCWB1T model hindcasts (cross-hatched bar). Red dots indicate the observed EAWM index of individual El Niño years (last two digits of each El Niño year are written to the left of each red dot). The values shown for the hindcasts are averaged from lead-0 to lead-5 month hindcasts, and the error bars represent one standard deviation among all the lead months.

1992/93, 2004/05, and 2009/10 events). We used these observed events for analysis in this study. Anomalies of the observational datasets and model hindcasts were calculated as departures from their monthly climatological values for the analysis period. To analyze the anomalies, a number of ordinary statistical methods such as composite, correlation, and regression analyses were carried out. A statistical significance was assessed using a two-tailed Student's *t* test. Unless otherwise stated, the boreal winter months of December, January, and February (i.e., DJF) were adopted as the main season of this study.

3. Results

a. EAWM responses to diverse El Niño types in the observations

We first examine the EAWM responses to diverse El Niño types in the observations by compositing the changes of the EAWM index during the EP, CP-I, and CP-II El Niño events. The solid bars in Fig. 1 indicate that the EAWM index has a negative value during all three types of El Niño. This means that the conventional view of the El Niño–EAWM relationship that El Niño weakens the intensity of EAWM is in operation regardless of the El Niño type. However, it is also evident that the degrees of the weakening effect are different among the three El Niño types. The EP El Niño has the strongest weakening effect on the EAWM, CP-II El Niño has the second strongest, and CP-I El Niño has the weakest. The averaged EAWM index value during the EP type (−1.41 s.d.) is approximately 2 times stronger than that of the CP-II type (−0.75 s.d.), while the index value during the CP-I type is only −0.17 s.d. (see Table 1). These results indicate that, although all three El Niño types exhibit the conventional El Niño–EAWM relationship, there are clear differences in the EAWM responses to the three types of El Niño. The individual El Niño years (delineated by red dots in Fig. 1) generally follow the above results, ensuring that the composite analysis results are reasonable despite the small degrees of freedom.

To understand the cause of the different EAWM responses to diverse El Niño types, we show in Fig. 2 the composite atmospheric structures of anomalous low-level wind and surface pressure for the three El Niño types. During the EP El Niño (Fig. 2a), the atmospheric structure is dominated by a strong anomalous anticyclone over the western North Pacific near the Philippine Sea, namely the WNPAC. As mentioned, the WNPAC can produce southerly wind anomalies to impair EAWM's northerly wind and is a key mechanism to drive the negative relation between El Niño and EAWM. Figure 2 shows that the WNPAC also appear in the atmosphere structures for the CP-I (Fig. 2b) and CP-II (Fig. 2c) El Niños but with smaller magnitudes. As shown in Table 1, the strength of WNPAC is about 2.52 hPa during the EP El Niño, 0.58 hPa during the CP-I El Niño, and 0.92 hPa during the CP-II El Niño. These different WNPAC strengths are one major reason why three types of El Niño cause different weakening impacts on the EAWM.

Besides the differences in WNPAC strengths, there is another major difference in the atmospheric structures among the three types of El Niño. That is, an extratropical anomalous anticyclone appears near the Kuroshio Extension (i.e., the KAC) during the EP and CP-II El Niños, but not during the CP-I El Niño (see Figs. 2a–c). Recent studies (Son et al. 2014; S. Kim et al. 2017; Gong et al. 2019) have shown that the KAC during El Niño mature winter significantly affects the East Asian climate via enhancing the influence of El Niño on the EAWM. Similar to the WNPAC, the KAC weakens the intensity of EAWM through an enhancement of southerly wind anomalies in its western flank, which impairs the climatological northerly wind over Northeast Asia including Japan, the Korean Peninsula, and northeastern China. In Figs. 2a and 2c, such pronounced southerly wind anomalies are seen blowing into Northeast Asia from the anomalous anticyclone near the Kuroshio Extension. The strength of KAC has positive values during the EP and CP-II El Niños but a weak negative value during the CP-I El Niño (see Table 1). Therefore, our results suggest that the EP El Niño produces the strongest weakening effect on the EAWM via both the WNPAC and KAC. The WNPAC and KAC both appear during the CP-II El Niño but with weaker circulation strengths than those appearing during the EP El Niño, enabling this El Niño type to result in the second strongest weakening effect on the EAWM. The WNPAC's weak strength and the absence of the KAC explain why the weakening effect of the CP-I El Niño on the EAWM is smallest among all three El Niño types. The stippling areas in Figs. 2a–c, where the composite surface pressure anomalies are statistically significant, further support the above suggestion.

b. The WNPAC and KAC impact mechanisms

In this section, we examine why diverse El Niño types produce different strengths of the WNPAC and KAC. The reasons for the different WNPAC strengths we find in this study are in general consistent with the results of Chen et al. (2019), where they examined the observed responses of the western

TABLE 1. Mean values of the EAWM index (s.d.), WNPAC index (hPa), and KAC index (hPa) in the observations (OBS) and the TCWB1T model hindcasts and their differences in percentage (relative to the observations; denoted as "Diff.") for the three types of EP, CP-I, and CP-II El Niño events. Values in parentheses in TCWB1T denote one standard deviation of the model hindcasts from all the lead months.

	EP El Niño			CP-I El Niño			CP-II El Niño		
	OBS	TCWB1T	Diff.	OBS	TCWB1T	Diff.	OBS	TCWB1T	Diff.
EAWM index	−1.41	−0.74 (0.27)	−47.5%	−0.17	−0.16 (0.21)	−5.9%	−0.75	−0.33 (0.16)	−56.0%
WNPAC index	2.52	1.82 (0.45)	−27.8%	0.58	0.52 (0.12)	−10.3%	0.92	0.91 (0.19)	−1.1%
KAC index	1.86	−0.54 (0.30)	−129%	−0.13	−0.32 (0.31)	−146%	0.26	−0.39 (0.17)	−250%

Pacific subtropical high to the three types of El Niño. Their results (see their Fig. 1) showed that, during El Niño mature winter, the western Pacific subtropical high (i.e., the WNPAC) response is much stronger during the EP type than the two CP types. They argued that the different WNPAC responses can be explained by an El Niño–induced Gill-type (Gill 1980) response mechanism proposed by C. Wang et al. (1999) and B. Wang et al. (2000). The anomalous diabatic heating induced by El Niño can excite a series of Gill responses and atmosphere–ocean coupling to impact the WNPAC. Since the warm SST anomalies of the EP El Niño are located far more into the tropical eastern Pacific (Fig. 3a), a two-step Gill response is needed to link the El Niño to the WNPAC. In the first step, the positive diabatic heating anomaly released by the El Niño–induced precipitation anomalies (Fig. 3d) excites an anomalous cyclone to the west of the anomalies. The cyclone brings an anomalous northeasterly on its western flank, enhancing the climatological trade winds to produce an anomalous cooling in the subtropical central Pacific. The cooling (i.e., negative diabatic heating anomaly) excites a second Gill response to induce an anomalous anticyclone over the western North Pacific, strengthening the WNPAC. In contrast, the warm SST anomalies and the related diabatic heating anomalies are systematically shifted westward and close to the tropical central Pacific during the two types of CP El Niño (Figs. 3b,c). Consequently, an anomalous cyclone, excited by the first step of the Gill response over the subtropical central Pacific, also migrates westward and appears near the western North Pacific, weakening the WNPAC as it occupies the area where the WNPAC develops. Therefore, the Gill-type response mechanism during both the CP-I and CP-II El Niños tends to weaken, rather than strengthen, the WNPAC.

In addition to this, we also suggest that the effect of Indian Ocean warming can be responsible for the different WNPAC responses during diverse El Niño types. El Niño events can lead to an anomalous warming in the Indian Ocean during their developing seasons through suppressing the atmospheric convection and the related shortwave radiative heating over the region via a change in the Walker circulation (cf. Klein et al. 1999; Lau and Nath 2003). The induced Indian Ocean warm anomaly maintains itself during the latter seasons and, in the meantime, helps strengthen the WNPAC by modulating the Walker circulation–related regional overturning circulations that further suppress the convection over the western North Pacific (e.g., Watanabe and Jin 2002, 2003; Kug and Kang 2006; Kug et al. 2006; J. W. Kim et al. 2017). As the composite surface pressure and precipitation anomalies displayed in Fig. 3 indicate, the EP El Niño induces a stronger anomalous Walker circulation than the CP-I and CP-II El Niños. Figures 3a–c also confirm that the composite warm SST anomalies in the Indian Ocean are stronger during the EP El Niño than during the two CP-type El Niños. Chen et al. (2019) showed that the Indian Ocean warming effect is weaker during the CP-I and CP-II El Niños than the EP El Niño.

Our analyses and the results from Chen et al. (2019) suggest that the processes of a Gill-type response and the Indian Ocean warming effect work constructively to enable the EP El Niño to produce a stronger strengthening impact on the WNPAC. However, during the CP-I and CP-II El Niños, the Gill response process produces a weakening impact on the WNPAC, and the strengthening effect from the Indian Ocean warming process is also weak. The different central locations of the warm SST anomalies are the ultimate reason why the EP El Niño can produce a stronger strengthening impact on the WNPAC than the two CP-type El Niños. In consequence, these different impacts on the WNPAC enable the EP El Niño to be more capable of weakening the intensity of EAWM than the two CP-type El Niños do.

We next move on to uncover the cause of the different KAC responses to diverse El Niño types. In Fig. 4a, we compute the correlation coefficients between the KAC index and tropical Pacific precipitation anomalies. The correlation pattern resembles the typical El Niño–induced precipitation anomalies with positive (negative) correlations in the eastern-to-central (western) tropical Pacific. It is also clear that the strongest correlations primarily appear in the northwestern tropical Pacific where negative correlations reside. This indicates that the anomalous negative precipitation forcing (i.e., negative diabatic heating anomaly) in the northwestern tropical Pacific plays a major role in exciting the KAC. The above arguments are further supported by a regression analysis. We compute regression coefficients of the anomalous atmospheric variables (i.e., low-level wind and surface pressure anomalies) with respect to a unit change of anomalous precipitation averaged in the northwestern tropical Pacific—namely the precipitation index. Here the precipitation index is defined as normalized boreal winter precipitation anomalies averaged over the selected northwestern tropical Pacific region (i.e., 0°–10°N, 130°–170°E; see rectangles in Fig. 4). This precipitation index was inversed, multiplied by −1, so that a positive index value corresponds to a negative precipitation anomaly (note that the main results were insensitive to any reasonable changes of the selected

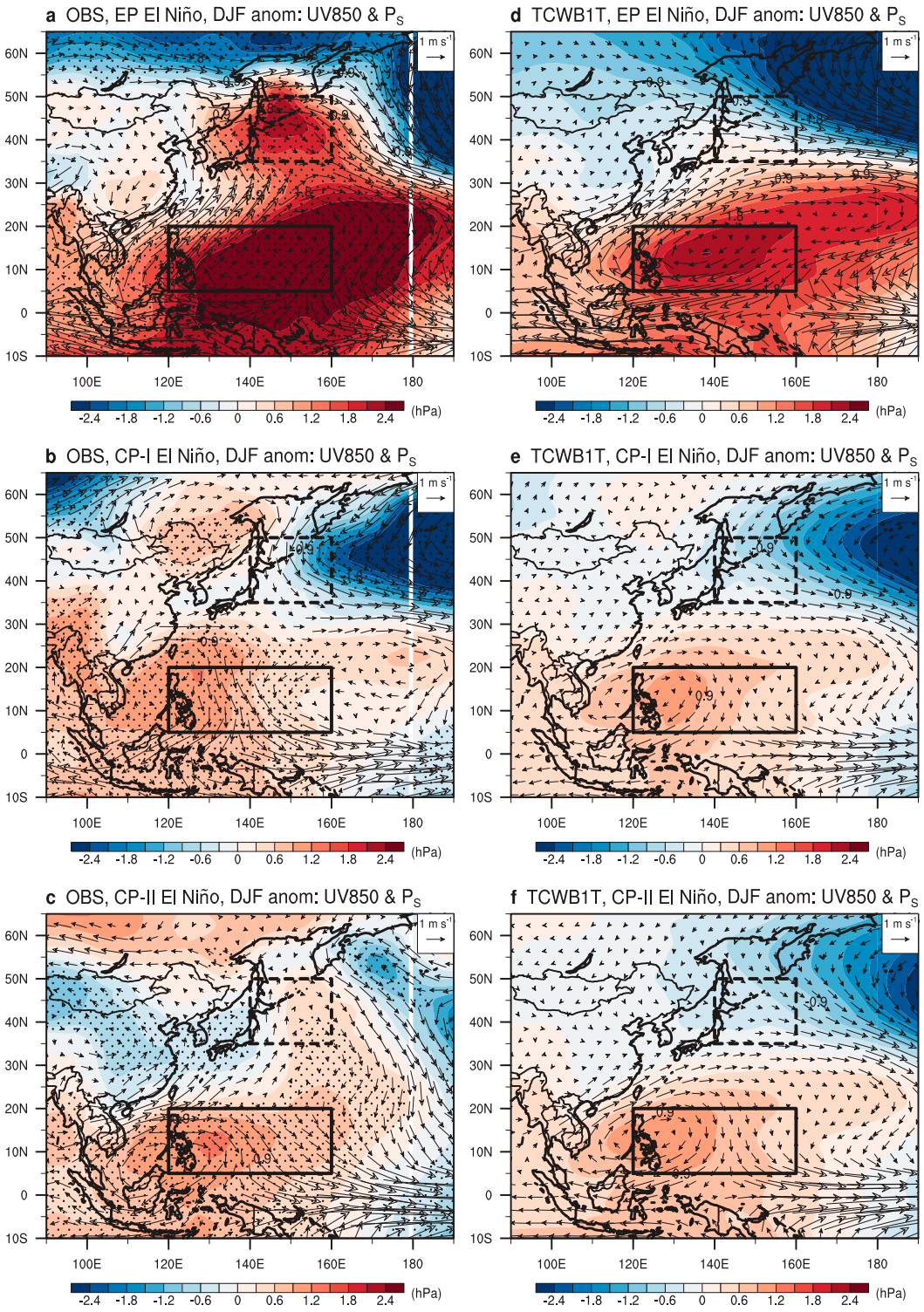

FIG. 2. Composite maps of anomalous low-level wind at 850-hPa level (UV850; vectors; m s^{-1}) and surface pressure (P_s; shading; hPa) during DJF for the (a) EP, (b) CP-I, and (c) CP-II El Niños from the observations (OBS). (d)–(f) As in (a)–(c), but for the TCWB1T model averaged from lead-0 to lead-5 month hindcasts. The solid (i.e., 5°–20°N, 120°–160°E) and dashed (i.e., 35°–50°N, 145°–165°E) rectangles denote the selected regions for quantifying strengths of the WNPAC and KAC, respectively. Stippling indicates areas where the composite surface pressure anomalies are statistically significant at the 90% confidence level according to a Student's t test.

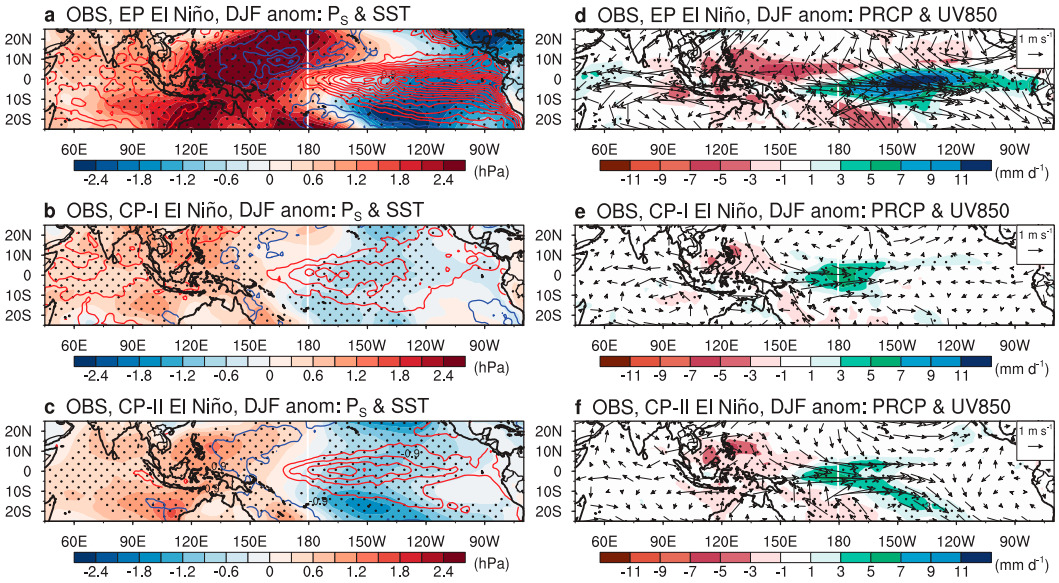

FIG. 3. Composite maps of anomalous surface pressure (P_s; shading; hPa) and sea surface temperature (SST; positive and negative values are expressed respectively as red and blue contours with 0.3°C interval) during DJF for (a) EP, (b) CP-I, and (c) CP-II El Niños from the observations (OBS). (d)–(f) As in (a)–(c), but for anomalous precipitation (PRCP; shading; mm day^{-1}) and low-level wind at the 850-hPa level (UV850; vectors; m s^{-1}). Stippling indicates areas where the composite values of anomalous surface pressure and precipitation are statistically significant at the 90% confidence level according to a Student's t test.

region). The inversed precipitation index-regressed atmospheric structure (Fig. 5a) shows an extratropical anomalous anticyclone near the Kuroshio Extension centered at 45°N and 150°E, namely the KAC. Previous studies (Son et al. 2014; S. Kim et al. 2017) have explained how the El Niño–induced negative precipitation anomalies over the northwestern tropical Pacific are critical to driving the KAC as follows. The strong negative diabatic heating anomaly released by the northwestern tropical Pacific negative precipitation anomalies induces an anomalous anticyclone in the lower troposphere (i.e., the WNPAC) and an anomalous cyclone in the upper troposphere. The upper-tropospheric divergence related to the anomalous cyclone excites a poleward atmospheric teleconnection pattern via a Rossby wave energy propagation, and subsequently produces an equivalently barotropic anomalous anticyclone near the Kuroshio Extension (i.e., the KAC).

As seen in Figs. 2a–c, the KAC can be excited during both the EP and CP-II El Niños but not the CP-I El Niño. We here suggest that there are two reasons for the absence of the KAC during the CP-I El Niño. First, the strength of negative precipitation anomalies in the northwestern tropical Pacific is weakest during the CP-I El Niño as compared to the EP and CP-II El Niños (Figs. 3d–f). Therefore, the anomalous diabatic forcing there that could excite the KAC is weak in the CP-I El Niño. Second, the anomalous cyclone over the North Pacific is largely shifted westward during the CP-I El Niño, close to the Kuroshio Extension, and induces anomalous northerly wind in the west of the cyclone (cf. Fig. 2b). These northerly wind anomalies can then effectively offset the KAC-associated southerly wind anomalies that would generally be capable of extending northward to 50°N of East Asia, as shown during the EP and CP-II El Niños (cf. Figs. 2a,c). Figure 6, which displays composite atmospheric structures for all three El Niño types using the Lambert conformal conic projection, supports the above suggestion. It is shown in Fig. 6b that the anomalous cyclone during the CP-I El Niño is largely shifted westward, west of the date line where the Aleutian low resides,

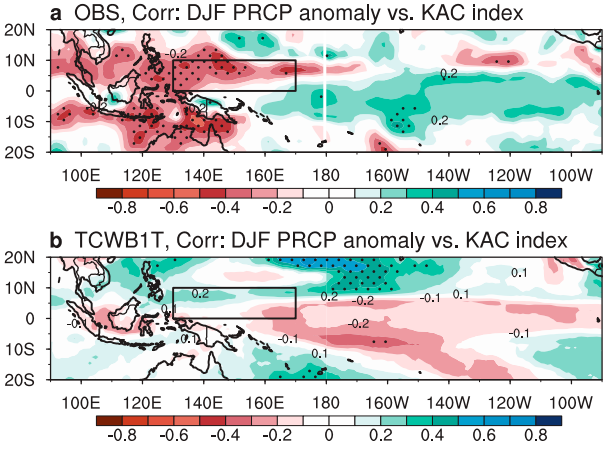

FIG. 4. Correlation maps of anomalous precipitation during DJF against the corresponding temporal variations of KAC index for the period 1982–2011 in (a) the observations (OBS) and (b) the TCWB1T model averaged from lead-0 to lead-5 month hindcasts. The solid rectangles denote the selected northwestern tropical Pacific region (i.e., 0°–10°N, 130°–170°E) for defining the precipitation index (cf. section 3b). Stippling indicates areas where the correlation coefficients are statistically significant at the 90% confidence level according to a Student's t test.

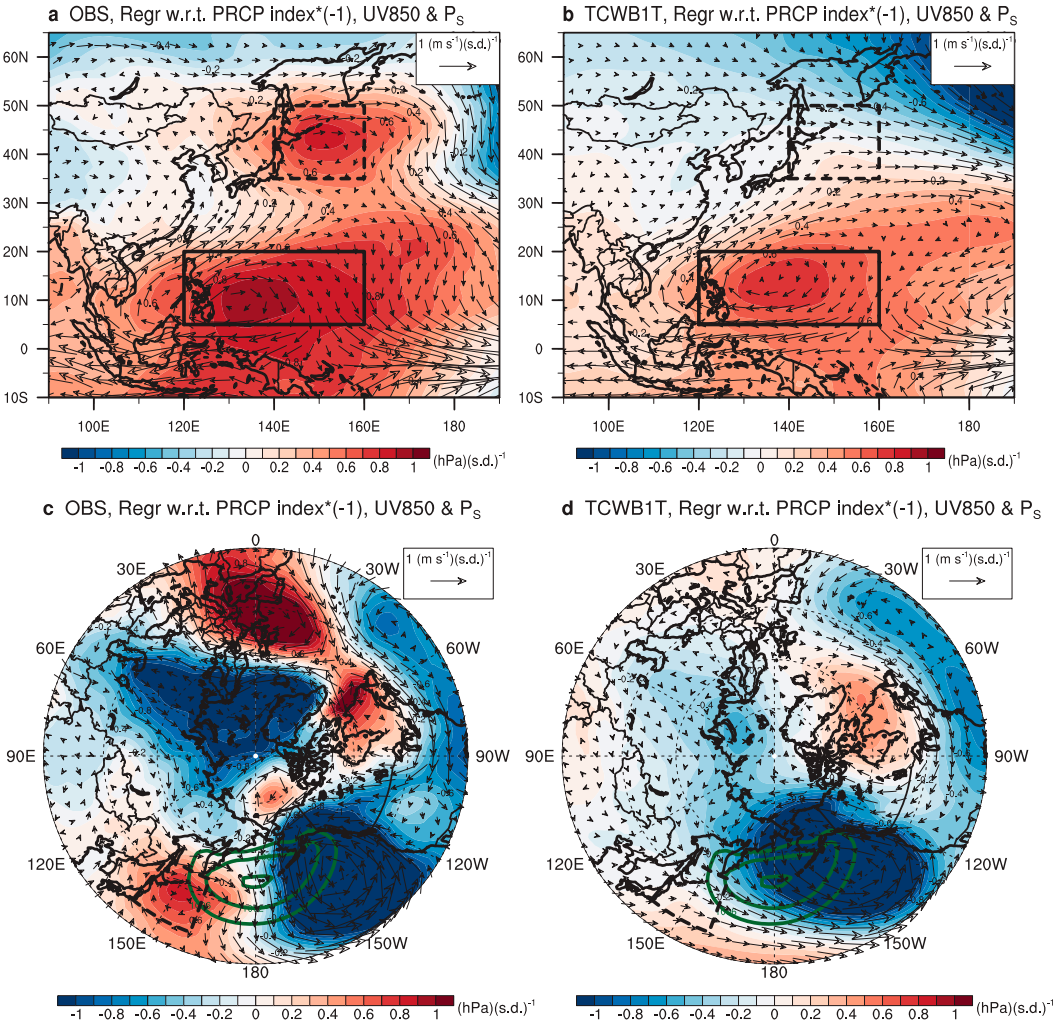

FIG. 5. Regression maps of anomalous low-level wind at the 850-hPa level (UV850; vectors; m s^{-1}) and surface pressure (P_s; shading; hPa) during DJF with respect to the inversed precipitation index (multiplied by −1; s.d.) for (a) the observations (OBS) and (b) the TCWB1T model averaged from lead-0 to lead-5 month hindcasts. (c),(d) As in (a) and (b), but using the polar stereographic projection in the Northern Hemisphere from 30° to 90°N. The green contours over the central North Pacific in (c) and (d) indicate the climatological location of the Aleutian low, which is depicted by raw surface pressure levels from 998 to 1006 hPa (4-hPa intervals). The solid and dashed areas are the selected region for the WNPAC and KAC in this study, respectively.

nearing the Kuroshio Extension (see green contours and dashed rectangles in Fig. 6). Note that this anomalous cyclone, which is the Aleutian low deepened by atmospheric teleconnection associated with El Niño, usually migrates southward, eastward, or southeastward from its normal position (cf. Horel and Wallace 1981). In contrast to the CP-I El Niño, the anomalous cyclones during the EP and CP-II El Niños (Figs. 6a,c) are moving away from the Kuroshio Extension and are shifted too far eastward or southeastward to hinder the occurrence of the KAC.

c. *EAWM responses to diverse El Niño types in the model hindcasts*

We extend our analysis to the TCWB1T model hindcasts to examine whether climate models can simulate the different EAWM responses to diverse El Niño types. By analyzing the lead-0 month hindcast, we find that the model reasonably simulates the climatological patterns of the EAWM-related wind and precipitation (Fig. 7a). Nevertheless, it is also seen that the model tends to overestimate precipitation levels over East Asia with 1–2 mm day^{-1} more than the observations (cf. shadings in Figs. 7a,b). This overall wet bias over East Asia is a common bias in simulations from contemporary coupled general circulation models (e.g., Gong et al. 2014; Wei et al. 2014). With relatively small differences in circulation field over East Asia (cf. vectors in Figs. 7a,b), the model accurately reproduces the observed EAWM-related climatological northerly wind generated by the strong horizontal pressure gradient between the Siberian high over the cold Eurasian continent and the

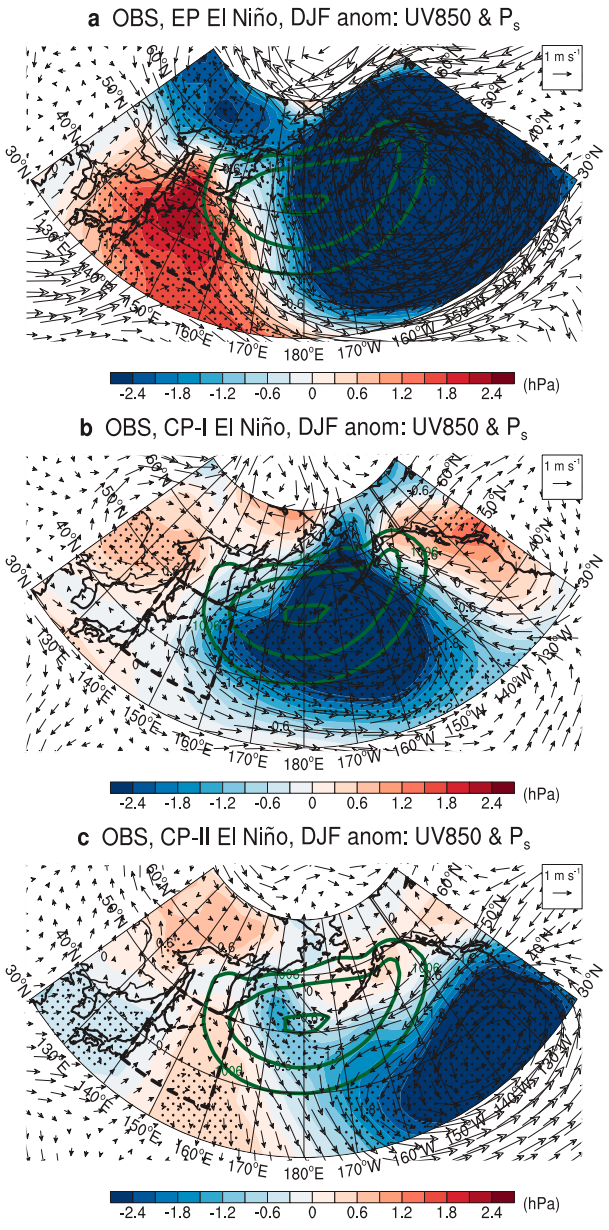

FIG. 6. Lambert conformal conic projection composite maps of anomalous low-level wind at the 850-hPa level (UV850; vectors; m s^{-1}) and surface pressure (P_s; shading; hPa) during DJF for (a) EP, (b) CP-I, and (c) CP-II El Niños from the observations (OBS). Stippling indicates areas where the composite surface pressure anomalies are statistically significant at the 90% confidence level according to a Student's *t* test. The green contours over the central North Pacific indicate the climatological location of the Aleutian low, which is depicted by raw surface pressure levels from 998 to 1006 hPa (4-hPa intervals). The dashed areas are the selected region for the KAC in this study.

Aleutian low over the warm Pacific Ocean. The model also realistically reproduces the observed seasonal change of the monsoonal winds over East Asia (Fig. 7c), showing a prevailing low-level northerly wind during the boreal cool season (i.e., October–March; blue shading in Fig. 7c) and a prevailing southerly wind during the boreal warm season (i.e., April–September).

We then compare the simulated EAWM responses to the three types of El Niño with the observations, which are seen in Fig. 1. It is found that the model generally follows the observed results with the order of strongest to weakest weakening effect on the EAWM, stemming from the EP, CP-II, and CP-I El Niños, respectively. However, it is also evident that the model underestimates the weakening effect, particularly for the EP and CP-II El Niños. During the EP and CP-II El Niños, the simulated EAWM index values are approximately 50% lower than those from the observations; the error ranges measured by one standard deviation also indicate that these underestimations are statistically significant (cf. Table 1). As revealed in the observational analysis, the diverse El Niños' impacts on the EAWM are established by altering the responses of WNPAC and KAC. Table 1 shows that the simulated WNPAC (KAC) index values are weaker than the observed by 27.8% (129%), 10.3% (146%), and 1.1% (250%) during the EP, CP-I, and CP-II El Niños, respectively. These model error values indicate that the model underestimates the WNPAC responses and completely fails (larger-than-100% differences) to produce the KAC responses to the three types of El Niño. The above results suggest that the model's largely underestimated weakening effect on the EAWM during the EP El Niño is related to both the WNPAC and KAC mechanisms, while that during the CP-II El Niño is only related to the KAC mechanism. The simulated WNPAC index value during the CP-II El Niño is close to the observed one (cf. Table 1).

Figure 2 shows that the WNPAC for the EP El Niño is notably weaker in the model hindcasts than in the observations (cf. Figs. 2a,d). For the CP-II El Niño, the model reasonably simulates the strength of WNPAC as well as its spatial structure (cf. Figs. 2c,f). For the CP-I El Niño, the model reproduces the observed location and strength of WNPAC, albeit with a slightly different structure from the observations (cf. Figs. 2b,e). The EP El Niño–induced precipitation anomalies in the model hindcasts (Fig. 8d) give a clue as to why the model underestimates the observed WNPAC strength during the EP El Niño. As compared to the observations (Fig. 3d), the simulated precipitation anomalies in the eastern-to-central tropical Pacific are considerably lower (Fig. 8d), despite the fact that the amplitude of simulated SST anomalies is similar to the observed one (Fig. 3a vs Fig. 8a). The diabatic heating anomalies associated with these weaker precipitation anomalies excite a weaker Gill response; thus, the model underestimates the observed WNPAC strength during the EP El Niño. Despite minor discrepancies, the model generally reproduces the observed precipitation anomalies concentrated toward the tropical central Pacific during the CP-I and CP-II El Niños (Figs. 3e,f vs Figs. 8e,f). Hence, they enable the model to simulate the WNPAC strengths close to the observations during the two CP-type El Niños.

Regarding the Indian Ocean warming effect, the model simulates a weaker Walker circulation anomaly than the observations during the EP El Niño, thereby inducing a weaker anomalous warming in the Indian Ocean (Fig. 3a vs Fig. 8a). The weakly induced Indian Ocean warm anomaly brings a weaker Indian Ocean warming effect than the observations, causing the model to underestimate the observed WNPAC

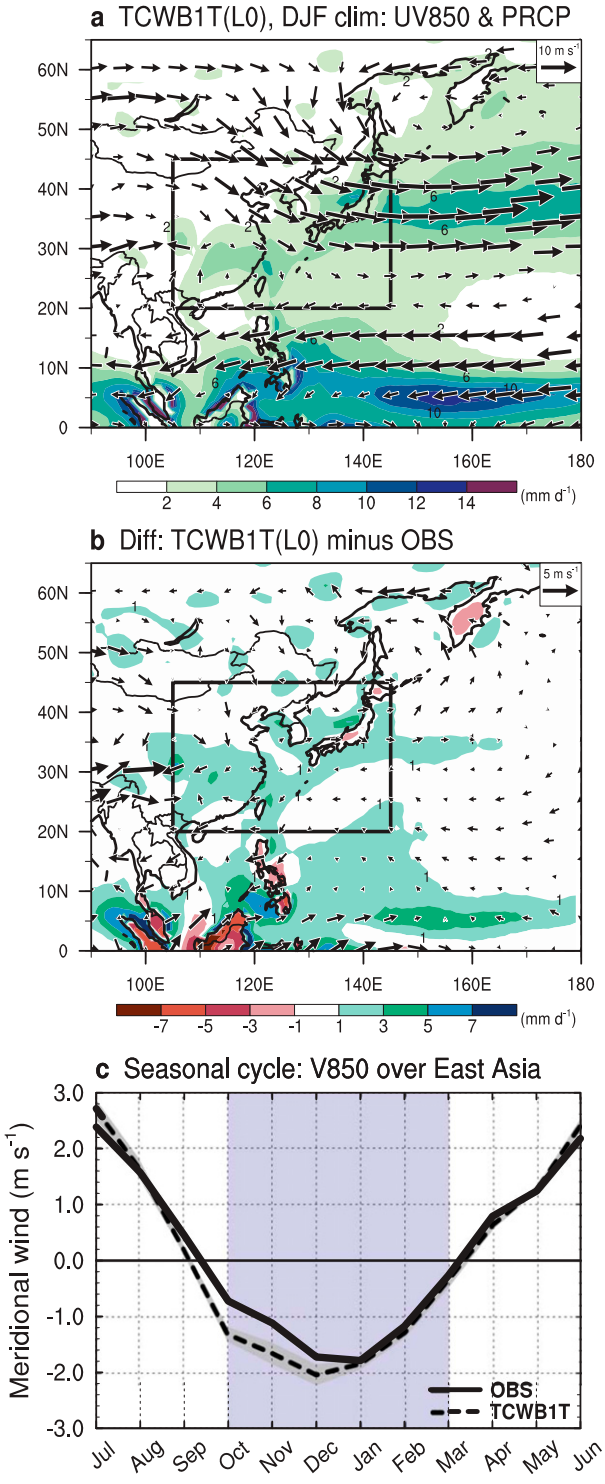

FIG. 7. Climatological pattern of low-level wind at the 850-hPa level (UV850; vectors; m s^{-1}) and precipitation (PRCP; shading; mm day^{-1}) during DJF for (a) the TCWB1T model at lead-0 month hindcast and (b) its difference from the observations (OBS) [i.e., TCWB1T(L0) minus OBS]. (c) Seasonal cycles of climatological low-level meridional wind (V850; m s^{-1}) averaged over the selected East Asian region [i.e., 20°–45°N and 105°–145°E; the rectangles in (a) and (b)] for the OBS (solid curve) and the TCWB1T model averaged from lead-0 to lead-5 month hindcasts (dashed curve) and their one standard deviations (gray shading). The blue shading in (c) indicates the boreal cool season from October to March.

strength during the EP El Niño. The model does not produce a noticeable anomalous warming in the Indian Ocean during the CP-I and CP-II El Niños (Figs. 8b,c), which is fairly consistent with the observations (Figs. 3b,c). Therefore, like the observations, the Indian Ocean warming effect in the model is also weak during the two CP-type El Niños.

The absence of a KAC response is a key factor explaining why the model underestimates the weakening effects on the EAWM during the EP and CP-II El Niños. Figure 2 shows that the observed KAC responses during the EP and CP-II El Niños are not reproduced in the model hindcasts. We venture to answer the question on why the model is unable to reproduce the observed KAC during El Niños. We already showed in the observational analysis that the KAC is resulted from an atmospheric wave train response to the negative precipitation anomalies over the northwestern tropical Pacific (Fig. 4a). We first repeat the same correlation analysis with the model hindcasts (Fig. 4b) and find that the correlations between the KAC index and tropical Pacific precipitation anomalies are mostly weak ($<\pm0.2$) and statistically insignificant over the tropics as compared to those in the observations. This indicates that the model cannot simulate the observed linkage between the KAC and the forcing from the El Niño. We next repeat the same regression analysis as in Fig. 5a except for the model hindcasts (Fig. 5b). Unlike the observational result, the regressed structure for the model hindcasts does not show any of the KAC-related atmospheric structure over the extratropics (cf. Figs. 5a,b). Therefore, a possible cause for the model's failure to simulate the KAC is the unrealistic response of the model's extratropical atmosphere to the negative diabatic heating anomaly in the northwestern tropical Pacific. The polar views displayed in Figs. 5c and 5d support this by showing that the model, in comparison to the observations, simulates an excessively expanded anomalous cyclone over the North Pacific that shifts far westward, covering the date line where the center of the Aleutian low is located (see green contours in Figs. 5c,d). This excessively expanded anomalous cyclone may hinder the formation of the KAC since it strengthens the midlatitude jet stream that enables the poleward propagating Rossby wave train to veer toward the east in the zonal direction, whereas the Rossby waves are normally expected to primarily propagate along the background jet stream in the midlatitude (cf. Hoskins et al. 1985).

4. Summary and discussion

In this study we have examined the varying responses of EAWM to three types of El Niño (i.e., EP, CP-I, and CP-II El Niño types) by analyzing the observational datasets and the retrospective hindcast simulations provided by the TCWB1T

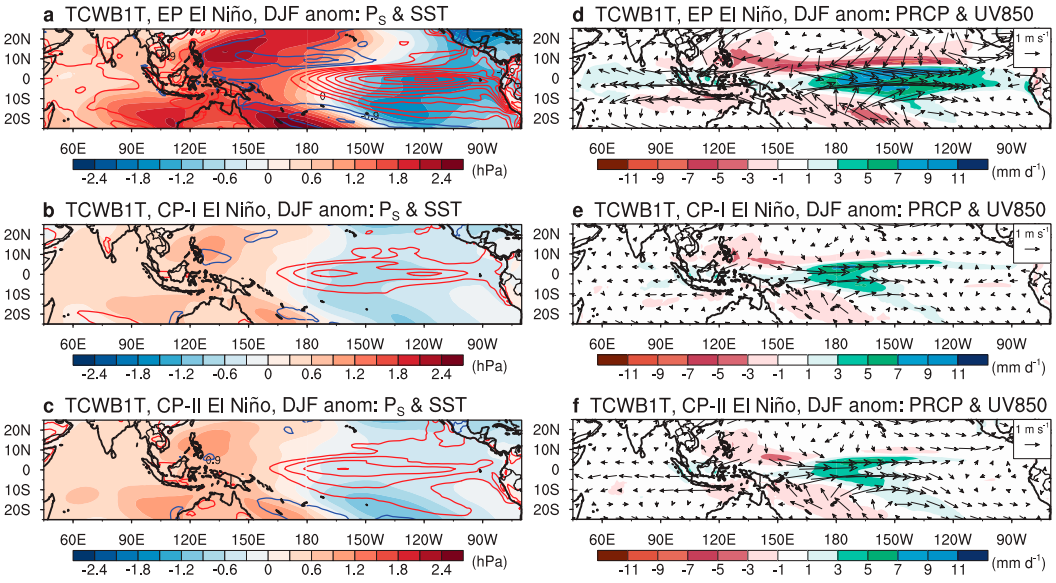

FIG. 8. Composite maps of anomalous surface pressure (P_s; shading; hPa) and SST (positive and negative values are expressed respectively as red and blue contours with 0.3°C interval) during DJF for (a) EP, (b) CP-I, and (c) CP-II El Niños from the TCWB1T model averaged from lead-0 to lead-5 month hindcasts. (d)–(f) As in (a)–(c), but for anomalous precipitation (PRCP; shading; mm day^{-1}) and low-level wind at the 850-hPa level (UV850; vectors; m s^{-1}).

model. This study has its own uniqueness from previous studies which mostly focused on the two types of EP and CP El Niños. The main findings of this study are summarized as follows:

- The observational analysis showed that the typical EAWM response to El Niño, which is characterized by the negative relation between El Niño and EAWM, dramatically changes among diverse El Niño types by disclosing the strongest weakening effect on the EAWM during the EP El Niño, the second strongest during the CP-II El Niño, and the least during the CP-I El Niño (Fig. 1 and Table 1). These varying EAWM responses to diverse El Niño types were controlled by the different responses of two anomalous anticyclones during El Niño mature winter, whose centers are located over the western North Pacific and the Kuroshio Extension, respectively termed the WNPAC and KAC in this study (Fig. 2 and Table 1).
- The different WNPAC responses to diverse El Niño types were explained via two physical processes of the Gill-type response mechanism and the Indian Ocean warming effect that respond to the El Niño–induced precipitation anomalies in the eastern-to-central tropical Pacific (Fig. 3). Meanwhile, the different KAC responses to diverse El Niño types were explained via the poleward propagating Rossby wave train that responds to the El Niño–induced precipitation anomalies in the northwestern tropical Pacific (Figs. 4, 5).
- The model analysis using the hindcast simulations similarly reproduced the observed weakening effect of three El Niño types on the EAWM. Nevertheless, an evident underestimation was also detected for the EP and CP-II El Niños (Fig. 1 and Table 1). These underestimations were directly linked to the model's simulation of a too-weak WNPAC response during the EP El Niño and completely failing to simulate a KAC response during the EP and CP-II El Niños (Fig. 2 and Table 1). The too-weak WNPAC response was attributed to the model's too-weak El Niño–induced precipitation anomalies in the eastern-to-central tropical Pacific (Fig. 8). The failure to simulate the KAC response was ascribed to the model's extratropical atmosphere that responds unrealistically to the El Niño–induced precipitation anomalies in the northwestern tropical Pacific (Figs. 4, 5).

While this study emphasized the different central locations of warm SST anomalies as an ultimate reason for why the EP El Niño can strengthen the WNPAC more than the two CP-type El Niños, it should also be noted that the different El Niño amplitudes between the EP- and CP-type events could play a role in impacting the WNPAC as they induce different magnitudes of negative diabatic heating anomalies over the western North Pacific. Furthermore, the small difference in WNPAC strength between the two CP-type El Niños is likely attributed to the negative diabatic heating anomalies (also, the cold SST anomalies) over the western North Pacific that are slightly stronger during the CP-II El Niño than the CP-I El Niño. These subtle but noticeable differences could drive different WNPAC strengths with greater intensity during CP-II El Niño but weaker intensity during CP-I El Niño. For this reason, alongside with the KAC that only appeared during CP-II El Niño, the different WNPAC strengths associated with CP-type El Niños can also contribute to the varying EAWM responses, leading to greater weakening of the EAWM during CP-II El Niño but more minor weakening during CP-I El Niño.

In addition to the unrealistic response of the model's extratropical atmosphere to the El Niño–induced negative

diabatic heating anomaly in the northwestern tropical Pacific (which we found in this study), another possible reason for its failure to simulate the KAC response is the model deficiency in simulating internal atmospheric circulation variability over the North Pacific, such as the overestimation of the Aleutian low magnitude. Most contemporary climate models have a systematic bias in reproducing the observed atmospheric circulation field over the North Pacific as they commonly overestimate the Aleutian low magnitude in their simulations (cf. Gong et al. 2016). It is also possible that the observed KAC response is forced by other basins, apart from the western Pacific Ocean, such as the tropical Indian Ocean or the southern Maritime Continent. Therefore, our conclusions regarding the model's failure to simulate the KAC response may require careful interpretation and further research.

Finally, although this study conducted the hindcast simulations from one specific TCWB1T1 model, the model deficiencies in simulating EAWM responses differently from the observations through different responses of the WNPAC and KAC (which we found in this study) can be shared with many other climate models. For instance, S. Kim et al. (2017) reported that climate models participating in phase 5 of the Coupled Model Intercomparison Project tend to underestimate the observed El Niño–induced tropical Pacific precipitation anomalies in boreal winter, thereby leading to weaker-than-observations atmospheric responses over the remote regions during the same season. As we have shown in this study, these underestimated tropical Pacific precipitation anomalies in climate models can have an influence on the impact mechanisms of WNPAC and KAC, in turn altering the EAWM responses during El Niño mature winter. In this context, the findings of this study are thus applicable to other climate models to improve prediction skills of EAWM and are of general interest to the climate research community.

Acknowledgments. The authors thank the three anonymous reviewers whose helpful suggestions and insightful comments improved this study greatly. The authors also appreciate D. Kang for his comments on interpreting the model hindcast results. This research was supported by a grant from Central Weather Bureau of Taiwan under Grant IISI-202924. J.-W. Kim and J.-Y. Yu are also supported by NSF Climate and Large-Scale Dynamics Program under Grant AGS-1833075. Authors appreciated all data providers, which can be found in the following addresses: NCEP-DOE R2 at https://www.esrl.noaa.gov/psd/data/gridded/data.ncep.reanalysis2.html, GPCPv2.3 at https://www.esrl.noaa.gov/psd/data/gridded/data.gpcp.html, and HadISSTv1.1 at https://www.metoffice.gov.uk/hadobs/.

REFERENCES

Adler, R. F., and Coauthors, 2003: The version-2 Global Precipitation Climatology Project (GPCP) monthly precipitation analysis (1979–present). *J. Hydrometeor.*, **4**, 1147–1167, https://doi.org/10.1175/1525-7541(2003)004<1147:TVGPCP>2.0.CO;2.

Alexander, M. A., I. Bladé, M. Newman, J. R. Lanzante, N. C. Lau, and J. D. Scott, 2002: The atmospheric bridge: The influence of ENSO teleconnections on air–sea interaction over the global oceans. *J. Climate*, **15**, 2205–2231, https://doi.org/10.1175/1520-0442(2002)015<2205:TABTIO>2.0.CO;2.

Ashok, K., S. K. Behera, S. A. Rao, H. Weng, and T. Yamagata, 2007: El Niño Modoki and its possible teleconnection. *J. Geophys. Res.*, **112**, C11007, https://doi.org/10.1029/2006JC003798.

Capotondi, A., and Coauthors, 2015: Understanding ENSO diversity. *Bull. Amer. Meteor. Soc.*, **96**, 921–938, https://doi.org/10.1175/BAMS-D-13-00117.1.

Chan, J. C., and C. Li, 2004: The East Asia winter monsoon. *East Asian Monsoon*, C.-P. Chang, Ed., World Scientific, 54–106.

Chang, C.-P., and K. M. Lau, 1982: Short-term planetary-scale interactions over the tropics and midlatitudes during northern winter. Part I: Contrasts between active and inactive periods. *Mon. Wea. Rev.*, **110**, 933–946, https://doi.org/10.1175/1520-0493(1982)110<0933:STPSIO>2.0.CO;2.

——, J. E. Erickson, and K. M. Lau, 1979: Northeasterly cold surges and near-equatorial disturbances over the winter MONEX area during December 1974. Part I: Synoptic aspects. *Mon. Wea. Rev.*, **107**, 812–829, https://doi.org/10.1175/1520-0493(1979)107<0812:NCSANE>2.0.CO;2.

——, Z. Wang, J. Ju, and T. Li, 2004: On the relationship between western Maritime Continent monsoon rainfall and ENSO during northern winter. *J. Climate*, **17**,665–672, https://doi.org/10.1175/1520-0442(2004)017<0665:OTRBWM>2.0.CO;2.

——, ——, and H. Hendon, 2006: The Asian winter monsoon. *The Asian Monsoon*, B. Wang, Ed., Springer, 89–127.

Chen, M., J. Y. Yu, X. Wang, and W. Jiang, 2019: The changing impact mechanisms of a diverse El Niño on the western Pacific subtropical high. *Geophys. Res. Lett.*, **46**, 953–962, https://doi.org/10.1029/2018GL081131.

——, T. H. Chang, C. T. Lee, S. W. Fang, and J. Y. Yu, 2020: A study of climate model responses of the western Pacific subtropical high to El Niño diversity. *Climate Dyn.*, **56**, 581–595, https://doi.org/10.1007/s00382-020-05500-2.

Chen, X., C. Li, J. Ling, and Y. Tan, 2017: Impact of East Asian winter monsoon on MJO over the equatorial western Pacific. *Theor. Appl. Climatol.*, **127**, 551–561, https://doi.org/10.1007/s00704-015-1649-x.

Ding, Y., 1994: *Monsoons over China*. Springer, 420 pp.

——, and T. N. Krishnamurti, 1987: Heat budget of the Siberian high and the winter monsoon. *Mon. Wea. Rev.*, **115**, 2428–2449, https://doi.org/10.1175/1520-0493(1987)115<2428:HBOTSH>2.0.CO;2.

Gill, A. E., 1980: Some simple solutions for heat-induced tropical circulation. *Quart. J. Roy. Meteor. Soc.*, **106**, 447–462, https://doi.org/10.1002/qj.49710644905.

Gong, H., L. Wang, W. Chen, R. Wu, K. Wei, and X. Cui, 2014: The climatology and interannual variability of the East Asian winter monsoon in CMIP5 models. *J. Climate*, **27**, 1659–1678, https://doi.org/10.1175/JCLI-D-13-00039.1.

——, ——, ——, D. Nath, G. Huang, and W. Tao, 2015: Diverse influences of ENSO on the East Asian–western Pacific winter climate tied to different ENSO properties in CMIP5 models. *J. Climate*, **28**, 2187–2202, https://doi.org/10.1175/JCLI-D-14-00405.1.

——, ——, ——, X. Chen, and D. Nath, 2016: Biases of the wintertime Arctic Oscillation in CMIP5 models. *Environ. Res. Lett.*, **12**, 014001, https://doi.org/10.1088/1748-9326/12/1/014001.

——, ——, and ——, 2019: Recently strengthened influence of ENSO on the wintertime East Asian surface air temperature. *Atmosphere*, **10**, 720, https://doi.org/10.3390/atmos10110720.

Horel, J. D., and J. M. Wallace, 1981: Planetary-scale atmospheric phenomena associated with the Southern Oscillation. *Mon.*

Wea. Rev., **109**, 813–829, https://doi.org/10.1175/1520-0493(1981)109<0813:PSAPAW>2.0.CO;2.

Hoskins, B. J., M. E. McIntyre, and A. W. Robertson, 1985: On the use and significance of isentropic potential vorticity maps. *Quart. J. Roy. Meteor. Soc.*, **111**, 877–946, https://doi.org/10.1002/qj.49711147002.

Huang, R., L. Zhou, and W. Chen, 2003: The progresses of recent studies on the variabilities of the East Asian monsoon and their causes. *Adv. Atmos. Sci.*, **20**, 55–69, https://doi.org/10.1007/BF03342050.

——, J. Chen, and G. Huang, 2007: Characteristics and variations of the East Asian monsoon system and its impacts on climate disasters in China. *Adv. Atmos. Sci.*, **24**, 993–1023, https://doi.org/10.1007/s00376-007-0993-x.

Ji, L., S. Sun, K. Arpe, and L. Bengtsson, 1997: Model study on the interannual variability of Asian winter monsoon and its influence. *Adv. Atmos. Sci.*, **14**, 1–22, https://doi.org/10.1007/s00376-997-0039-4.

Kanamitsu, M., W. Ebisuzaki, J. Woollen, S. K. Yang, J. J. Hnilo, M. Fiorino, and G. L. Potter, 2002: NCEP–DOE AMIP-II reanalysis (R-2). *Bull. Amer. Meteor. Soc.*, **83**, 1631–1644, https://doi.org/10.1175/BAMS-83-11-1631.

Kang, D., and M. I. Lee, 2019: ENSO influence on the dynamical seasonal prediction of the East Asian winter monsoon. *Climate Dyn.*, **53**, 7479–7495, https://doi.org/10.1007/s00382-017-3574-4.

Kao, H. Y., and J. Y. Yu, 2009: Contrasting eastern-Pacific and central-Pacific types of ENSO. *J. Climate*, **22**, 615–632, https://doi.org/10.1175/2008JCLI2309.1.

Kim, J.-W., and S.-I. An, 2019: Western North Pacific anticyclone change associated with the El Niño–Indian Ocean dipole coupling. *Int. J. Climatol.*, **39**, 2505–2521, https://doi.org/10.1002/joc.5967.

——, S.-W. Yeh, and E.-C. Chang, 2014: Combined effect of El Niño–Southern Oscillation and Pacific decadal oscillation on the East Asian winter monsoon. *Climate Dyn.*, **42**, 957–971, https://doi.org/10.1007/s00382-013-1730-z.

——, S.-I. An, S.-Y. Jun, H.-J. Park, and S.-W. Yeh, 2017: ENSO and East Asian winter monsoon relationship modulation associated with the anomalous northwest Pacific anticyclone. *Climate Dyn.*, **49**, 1157–1179, https://doi.org/10.1007/s00382-016-3371-5.

Kim, S., H. Y. Son, and J. S. Kug, 2017: How well do climate models simulate atmospheric teleconnctions over the North Pacific and East Asia associated with ENSO? *Climate Dyn.*, **48**, 971–985, https://doi.org/10.1007/s00382-016-3121-8.

Klein, S. A., B. J. Soden, and N. C. Lau, 1999: Remote sea surface temperature variations during ENSO: Evidence for a tropical atmospheric bridge. *J. Climate*, **12**, 917–932, https://doi.org/10.1175/1520-0442(1999)012<0917:RSSTVD>2.0.CO;2.

Kug, J.-S., and I.-S. Kang, 2006: Interactive feedback between ENSO and the Indian Ocean. *J. Climate*, **19**, 1784–1801, https://doi.org/10.1175/JCLI3660.1.

——, B. P. Kirtman, and I.-S. Kang, 2006: Interactive feedback between ENSO and the Indian Ocean in an interactive ensemble coupled model. *J. Climate*, **19**, 6371–6381, https://doi.org/10.1175/JCLI3980.1.

——, F.-F. Jin, and S.-I. An, 2009: Two types of El Niño events: Cold tongue El Niño and warm pool El Niño. *J. Climate*, **22**, 1499–1515, https://doi.org/10.1175/2008JCLI2624.1.

Lau, K. M., and M. T. Li, 1984: The monsoon of East Asia and its global associations—A survey. *Bull. Amer. Meteor. Soc.*, **65**, 114–125, https://doi.org/10.1175/1520-0477(1984)065<0114:TMOEAA>2.0.CO;2.

Lau, N. C., and M. J. Nath, 2003: Atmosphere–ocean variations in the Indo-Pacific sector during ENSO episodes. *J. Climate*, **16**, 3–20, https://doi.org/10.1175/1520-0442(2003)016<0003:AOVITI>2.0.CO;2.

Li, T., B. Wang, B. Wu, T. Zhou, C. P. Chang, and R. Zhang, 2017: Theories on formation of an anomalous anticyclone in western North Pacific during El Niño: A review. *J. Meteor. Res.*, **31**, 987–1006, https://doi.org/10.1007/s13351-017-7147-6.

Li, X. Z., 1955: A study of cold waves in East Asia. *Meteorology (1919–1949)*, Offprints of Scientific Works in Modern China Series, Science Press, 35–117.

Ma, T., W. Chen, D. Nath, H. F. Graf, L. Wang, and J. Huangfu, 2018: East Asian winter monsoon impacts the ENSO-related teleconnections and North American seasonal air temperature prediction. *Sci. Rep.*, **8**, 6547, https://doi.org/10.1038/s41598-018-24552-3.

McPhaden, M. J., S. E. Zebiak, and M. H. Glantz, 2006: ENSO as an integrating concept in Earth science. *Science*, **314**, 1740–1745, https://doi.org/10.1126/SCIENCE.1132588.

Newman, M., and P. D. Sardeshmukh, 1998: The impact of the annual cycle on the North Pacific/North American response to remote low-frequency forcing. *J. Atmos. Sci.*, **55**, 1336–1353, https://doi.org/10.1175/1520-0469(1998)055<1336:TIOTAC>2.0.CO;2.

Pacanowski, R. C., and S. M. Griffies, 1998: MOM 3.0 manual. Geophysics Fluid Dynamics Laboratory, 708 pp.

Paek, H., J. Y. Yu, J. W. Hwu, M. M. Lu, and T. Gao, 2015: A source of AGCM bias in simulating the western Pacific subtropical high: Different sensitivities to the two types of ENSO. *Mon. Wea. Rev.*, **143**, 2348–2362, https://doi.org/10.1175/MWR-D-14-00401.1.

Rayner, N. A., D. E. Parker, E. B. Horton, C. K. Folland, L. V. Alexander, D. P. Rowell, E. C. Kent, and A. Kaplan, 2003: Global analyses of sea surface temperature, sea ice, and night marine air temperature since the late nineteenth century. *J. Geophys. Res.*, **108**, 4407, https://doi.org/10.1029/2002JD002670.

Sakai, K., and R. Kawamura, 2009: Remote response of the East Asian winter monsoon to tropical forcing related to El Niño–Southern Oscillation. *J. Geophys. Res.*, **114**, D06105, https://doi.org/10.1029/2008JD010824.

Shi, J., and W. Qian, 2018: Asymmetry of two types of ENSO in the transition between the East Asian winter monsoon and the ensuing summer monsoon. *Climate Dyn.*, **51**, 3907–3926, https://doi.org/10.1007/s00382-018-4119-1.

Son, H. Y., J. Y. Park, J. S. Kug, J. Yoo, and C. H. Kim, 2014: Winter precipitation variability over Korean Peninsula associated with ENSO. *Climate Dyn.*, **42**, 3171–3186, https://doi.org/10.1007/s00382-013-2008-1.

Tan, W., X. Wang, W. Wang, C. Wang, and J. Zuo, 2016: Different responses of sea surface temperature in the South China Sea to various El Niño events during boreal autumn. *J. Climate*, **29**, 1127–1142, https://doi.org/10.1175/JCLI-D-15-0338.1.

Tao, S. Y., 1957: A study of activities of cold air in East Asian winter. *Handbook of Short-Term Forecast* (in Chinese), China Meteorological Administration, 60–92.

Wang, B., 2006: *The Asian Monsoon*. Springer Science & Business Media, 845 pp.

——, and Q. Zhang, 2002: Pacific–East Asian teleconnection. Part II: How the Philippine Sea anomalous anticyclone is established during El Niño development. *J. Climate*, **15**, 3252–3265, https://doi.org/10.1175/1520-0442(2002)015<3252:PEATPI>2.0.CO;2.

——, R. Wu, and X. Fu, 2000: Pacific–East Asian teleconnection: How does ENSO affect East Asian climate? *J. Climate*, **13**, 1517–1536, https://doi.org/10.1175/1520-0442(2000)013<1517:PEATHD>2.0.CO;2.

——, Z. Wu, C. P. Chang, J. Liu, J. Li, and T. Zhou, 2010: Another look at interannual-to-interdecadal variations of the East Asian winter monsoon: The northern and southern temperature modes. *J. Climate*, **23**, 1495–1512, https://doi.org/10.1175/2009JCLI3243.1.

Wang, C., and X. Wang, 2013: Classifying El Niño Modoki I and II by different impacts on rainfall in southern China and typhoon tracks. *J. Climate*, **26**, 1322–1338, https://doi.org/10.1175/JCLI-D-12-00107.1.

——, R. H. Weisberg, and J. I. Virmani, 1999: Western Pacific interannual variability associated with the El Niño–Southern Oscillation. *J. Geophys. Res.*, **104**, 5131–5149, https://doi.org/10.1029/1998JC900090.

Wang, X., and C. Wang, 2014: Different impacts of various El Niño events on the Indian Ocean Dipole. *Climate Dyn.*, **42**, 991–1005, https://doi.org/10.1007/s00382-013-1711-2.

Watanabe, M., and F.-F. Jin, 2002: Role of Indian Ocean warming in the development of Philippine Sea anticyclone during ENSO. *Geophys. Res. Lett.*, **29**, 1478, https://doi.org/10.1029/2001GL014318.

——, and ——, 2003: A moist linear baroclinic model: Coupled dynamical–convective response to El Niño. *J. Climate*, **16**, 1121–1139, https://doi.org/10.1175/1520-0442(2003)16<1121:AMLBMC>2.0.CO;2.

Wei, K., T. Xu, Z. Du, H. Gong, and B. Xie, 2014: How well do the current state-of-the-art CMIP5 models characterise the climatology of the East Asian winter monsoon? *Climate Dyn.*, **43**, 1241–1255, https://doi.org/10.1007/s00382-013-1929-z.

Wu, T. Y., H. M. H. Juang, Y. L. Chen, P. Y. Liu, S. I. Lin, J. H. Chen, and M. M. Lu, 2019: CWB CFS 1-Tier Hindcast Analysis and Forecast Verification. *43rd NOAA Annual Climate Diagnostics and Prediction Workshop*, Santa Barbara, CA, NOAA's National Weather Service, https://www.weather.gov/images/sti/climate/STIP/43CDPW/posters/T-YWu.jpg.

Yang, S., K. M. Lau, and K. M. Kim, 2002: Variations of the East Asian jet stream and Asian–Pacific–American winter climate anomalies. *J. Climate*, **15**, 306–325, https://doi.org/10.1175/1520-0442(2002)015<0306:VOTEAJ>2.0.CO;2.

Yeh, S. W., J. S. Kug, B. Dewitte, M. H. Kwon, B. P. Kirtman, and F.-F. Jin, 2009: El Niño in a changing climate. *Nature*, **461**, 511–514, https://doi.org/10.1038/nature08316.

Yu, J. Y., and H. Y. Kao, 2007: Decadal changes of ENSO persistence barrier in SST and ocean heat content indices: 1958–2001. *J. Geophys. Res.*, **112**, D13106, https://doi.org/10.1029/2006JD007654.

——, M. M. Lu, and S. T. Kim, 2012a: A change in the relationship between tropical central Pacific SST variability and the extratropical atmosphere around 1990. *Environ. Res. Lett.*, **7**, 034025, https://doi.org/10.1088/1748-9326/7/3/034025.

——, Y. Zou, S. T. Kim, and T. Lee, 2012b: The changing impact of El Niño on US winter temperatures. *Geophys. Res. Lett.*, **39**, L15702, https://doi.org/10.1029/2012GL052483.

——, X. Wang, S. Yang, H. Paek, and M. Chen, 2017: *The Changing El Niño–Southern Oscillation and Associated Climate Extremes*. John Wiley & Sons, Inc., 38 pp.

Yuan, Y., S. Yang, and Z. Zhang, 2012: Different evolutions of the Philippine Sea anticyclone between the eastern and central Pacific El Niño: Possible effects of Indian Ocean SST. *J. Climate*, **25**, 7867–7883, https://doi.org/10.1175/JCLI-D-12-00004.1.

Zhang, R., A. Sumi, and M. Kimoto, 1996: Impact of El Niño on the East Asian monsoon. *J. Meteor. Soc. Japan*, **74**, 49–62, https://doi.org/10.2151/jmsj1965.74.1_49.